A New Single End Wideband Impedance Based Fault Location Scheme for Distribution Systems

F. M. Aboshady[a,b,*], D. W. P. Thomas[a], Mark Sumner[a]

[a]*Department of Electrical and Electronic Engineering, University of Nottingham, Nottingham, UK*
[b]*Electrical Power and Machines Engineering Department, Tanta University, Tanta, Egypt*

Abstract

This paper proposes an improved impedance based fault location scheme based on system analysis at non-fundamental frequencies. The fault is treated as a voltage source that injects high frequency components into the system and the analysis is carried out using these injected components. The proposed method only requires local measurements at the substation and therefore is classified as a single end method. The new contribution is that the proposed method uses the distributed parameter line model to account for inductive and capacitive effects of the line. It has been evaluated on the IEEE 34-bus feeder which is based on an actual distribution system which has the typical features such as non-homogeneous feeder sections, asymmetrical line configurations, unbalanced loads and single and three-phase laterals. The fault point, fault resistance and fault inception angle have been varied to check their influence on the accuracy of the method. The simulation results demonstrate the accuracy of the proposed method where for most cases, the error in fault location is less than 50 m.

Keywords: fault location, fault transient, impedance based, single end

1. Introduction

The ability to maintain a reliable and robust electricity supply is becoming more and more challenged as the renewable energy sources replace the conventional generation and with the increasing electrification of transport and heating systems [1]. Faults must be detected,

*Corresponding author
Email addresses: fathy.aboshady@nottingham.ac.uk (F. M. Aboshady), dave.thomas@nottingham.ac.uk (D. W. P. Thomas), mark.sumner@nottingham.ac.uk (Mark Sumner)

located and repaired quickly to minimise system down-time and repair costs [2]. It is also useful to locate temporary faults so that the preventative maintenance can be undertaken before large-scale faults occur [2].

Fault location methods for distribution systems tend to be classified into impedance based [3–6], sparse measurements based [7], travelling wave based [8, 9], learning based [10] and integrated methods [11, 12] as discussed in [13]. For the impedance methods, measurements of the voltages and currents at the fundamental frequency are used to estimate the impedance/distance to the fault using single or multiple measurement point(s). Impedance based methods are low-cost and more suited to distribution systems [5] and a comparison between different impedance based techniques is presented in [14]. The common problem with this category is that several estimated fault locations can be created ("multiple estimation") due to the existence of laterals and branches in the distribution systems [13].

Modern distribution systems will be equipped with instruments such as smart meters and phasor measurement units. Sparse measurements methods use the devices installed along the entire system for fault location. In [7], the voltage data collected from different meters is used to assess voltage sags across the system and locate the fault. Alternatively, the fault inception creates waves that travel between the fault point and the system terminals. These travelling waves are used to locate the fault point based on relating the fault distance to the travelling time [8, 9]. Travelling wave based methods can be very accurate but require high sampling rates e.g. 1 MHz in [9]. Also, the presence of laterals and branches in distribution systems increases the implementation complexity. Learning based methods employ artificial intelligence such artificial neural networks (ANN) [10]. After training the algorithm offline, ANNs can be generalized to locate any fault case. However, a huge amount of training data is usually necessary, and retraining is required whenever the system configuration changes.

The integration of different methods helps to overcome the individual shortfalls such as the multiple estimation problem when using the single end impedance based methods. For example in [11], after applying an impedance based method to estimate the candidate fault points, information from smart meters is used to build a low voltage zone noting that the fault causes the highest drop in voltage at the fault zone. The high frequency transients generated

by the fault have also been used to establish "wideband" impedance based techniques that work at non-fundamental frequencies [15–19]—unlike traditional impedance based methods that use fundamental frequency analysis. This high frequency analysis means that the method requires only a short period of data. Therefore, the wideband analysis can be adapted to locate intermittent faults as well as permanent faults.

In [15, 16], single end and double end wideband impedance based techniques have been developed for a simple system with only one load at the end of the line. Both inductive and capacitive coupling were ignored as the line length was only 20 m. The single end method in [15] has been extended in [17] to be applicable to a complex distribution system with loading taps and distributed generation. However, the extension also ignored the effect of inductive coupling and the capacitance of the lines and a sampling rate of 50 kHz was used for data capture. In [17], the fault is treated as a virtual voltage source located at the fault point—a step change at the fault instant equal and opposite to the pre-fault voltage at the fault point. However, the paper does not present a specific algorithm to detect the fault inception instant. A double end method that uses synchronized measurements at both feeder ends and considers inductive coupling and capacitance of the lines has been presented in [18, 19]. From [15–19], it can be concluded that the wideband impedance based approach can be a viable technique, but further research is required to adapt it to large and complex distribution systems.

In this paper, a single end wideband impedance based fault location (SEWIBFL) scheme is presented that requires measurements at the substation only. The proposed method has been derived by considering the distributed parameter model of a distribution line to account for both the inductive and capacitive effects of real distribution lines (which are usually ignored). To the authors' best knowledge, the impedance based methods in the literature approximate the line model to a π circuit except in [3]. However, [3] is only valid for symmetrical and perfectly transposed lines. The proposed method is the first single end wideband impedance based method that uses the distributed parameter model for the lines and also considers an asymmetric line configuration. The proposed method uses a sample rate of 20 kHz and a short data window of 40 ms. Two algorithms are presented to detect the fault inception point, required for creating the virtual voltage source at the fault point. A new third order equation

is derived to estimate the fault distance for ground and phase faults. The proposed method is evaluated on the IEEE 34-bus distribution feeder that exhibits non-homogeneous feeder sections, unbalanced load together with single and three-phase lines [20].

The paper is organized as follows: in section 2, the new fault location formula is derived for both ground and phase faults. The application of the method to a real distribution system is presented in section 3. In section 4, algorithms to precisely detect the fault inception point are presented. Section 5 provides the simulation studies on the IEEE 34-bus feeder, and finally, section 6 concludes the paper and describes where future work may be directed.

2. Proposed SEWIBFL scheme

The single end wideband impedance based fault location (SEWIBFL) scheme is presented in this section for a point to point system i.e. a single section system. The proposed method uses the distributed parameter line model to account for the inductive and capacitive effects of the lines. For a line with a per unit length series impedance and shunt admittance of Z_l and Y_l respectively, the equivalent distributed parameter line model is shown in Fig. 1. The voltage and current at a distance x from the sending node S can be calculated using (1) [21].

$$\begin{bmatrix} V_x \\ I_x \end{bmatrix} = \begin{bmatrix} \cosh(\gamma x) & -z_c \sinh(\gamma x) \\ -\sinh(\gamma x)/z_c & \cosh(\gamma x) \end{bmatrix} \begin{bmatrix} V_S \\ I_S \end{bmatrix} \tag{1}$$

where γ and z_c are the propagation constant and characteristic impedance of the line respectively and are given by (2)

$$\gamma = \sqrt{Z_l Y_l}\ ,\ z_c = \sqrt{Z_l / Y_l} \tag{2}$$

For a three-phase system, Z_l and Y_l are 3×3 matrices with non zero off diagonal elements. In order to decouple the three phases to three independent modes, modal transformation can be used [2]. For symmetrical lines, the Clarke's transformation matrix is commonly used to transform between phase and modal domains. However, for an asymmetrical line, different transformation matrices for voltage and current are necessary and are calculated based on eigenvectors for $Z_l Y_l$ and $Y_l Z_l$ respectively [2]. This paper only considers the symmetrical line

case. In the modal domain, the propagation modes are referred to as α, β and 0. Equations (1) and (2) are applied for the three modes to calculate voltage and current at a distance x from the sending node S. The voltage and current can be transformed back to the phase domain if necessary. In the following subsections, the SEWIBFL scheme will be derived for both ground and phase faults. Clarke's transformation matrix is defined as (3) [2]:

$$T_{cl} = \begin{bmatrix} -1/\sqrt{6} & 2/\sqrt{6} & -1/\sqrt{6} \\ 1/\sqrt{2} & 0 & -1/\sqrt{2} \\ 1/\sqrt{3} & 1/\sqrt{3} & 1/\sqrt{3} \end{bmatrix} \tag{3}$$

such that $V_{modal\ domain} = T_{cl} V_{phase\ domain}$ and an equivalent equation can be written for current.

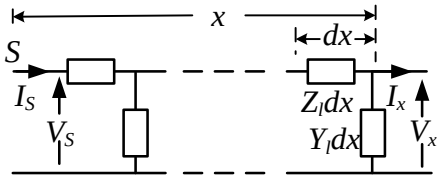

Fig. 1: Distributed parameter line

2.1. SEWIBFL scheme for a ground fault

Consider a system with a fault to ground as shown in Fig. 2a. The SEWIBFL scheme employs circuit analysis at non-fundamental frequencies to calculate the fault distance x measured from node S. The equivalent circuit at non-fundamental frequencies is illustrated in Fig. 2b where the supply voltage source V_{source} Thevenin equivalent is a short circuit and the fault is represented by a voltage source V_{fault}. Z_{eq} represents the equivalent impedance beyond the fault section. The fault voltage source is considered to be a step change which is equal to and opposite to the pre-fault voltage at the fault point [17]. This source injects a wideband of frequencies into the system. The circuit is analysed at these injected frequencies. To help understating the method, the procedure is divided into three stages which are:

1. Building the fault voltage source (V_{fault}) 2. Estimating the fault current

3. Estimating the fault distance

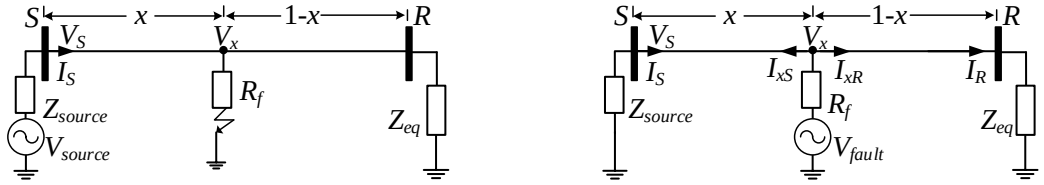

(a) at fundamental frequency

(b) at non-fundamental frequencies

Fig. 2: SEWIBFL scheme with ground fault

2.1.1. Building the fault voltage source

The pre-fault voltage (V_{Spre}) and current (I_{Spre}) at node S are used to calculate the pre-fault voltage at the fault point (V_{xpre}) using (4). Then, the fault voltage source (V_{fault}) is created as a step voltage source with a step change which is equal to and opposite to the pre-fault voltage at the fault point. After building V_{fault} in the time domain, its frequency spectrum can be obtained and used for the analysis of the next stages.

$$V_{xpre} = \cosh(\gamma x)V_{Spre} - z_c \sinh(\gamma x)I_{Spre} \tag{4}$$

2.1.2. Estimating the fault current

By analysing the circuit in Fig. 2b, the voltage and current at the fault point can be obtained using (1) where I_x in (1) is opposite to I_{xS} (the portion of the fault current flowing to the sending end). Then, V_x is used to calculate the load side current I_R using (5). The fault current is obtained through (6) and (7). Note that an estimate of Z_{eq} is required.

$$V_x = \{\cosh(\gamma(1-x))Z_{eq} + z_c \sinh(\gamma(1-x))\}I_R \tag{5}$$

$$I_{xR} = \{\sinh(\gamma(1-x))Z_{eq}/z_c + \cosh(\gamma(1-x))\}I_R \tag{6}$$

$$I_f = I_{xS} + I_{xR} \tag{7}$$

The first two stages of the procedure assume that x is known. Therefore, for the first iteration, an initial value for x is required and is assumed to be 0.01 pu. A new value for x is estimated and is used for the next iteration as discussed in section 2.1.3.

2.1.3. Estimating the fault distance

From (1), using the first two terms of the Taylor expansion for both $\cosh(\gamma x)$ and $\sinh(\gamma x)$, the voltage at the fault point (V_x) can be given by (8).

$$V_{x_j} = A_j + B_j x + C_j x^2 + D_j x^3 \tag{8}$$

where j refers to the propagation modes ($\alpha\beta 0$) and the coefficient values are given as follow:

$$A_j = V_{S_j} \qquad B_j = -\gamma_j z_{c_j} I_{S_j} \qquad C_j = \gamma_j^2 V_{S_j}/2 \qquad D_j = -\gamma_j^3 z_{c_j} I_{S_j}/6$$

From (8), the voltage V_x can be expressed in the *abc* domain by (9)

$$V_{x_{abc}} = T_{cl}^{-1} V_{x_{\alpha\beta 0}} = A_{abc} + B_{abc} x + C_{abc} x^2 + D_{abc} x^3 \tag{9}$$

where $K_{abc} = T_{cl}^{-1} K_{\alpha\beta 0}$, $K_{abc} = [K_a;\ K_b;\ K_c]$, T_{cl}^{-1} is the inverse Clarke's transform and K refers to A, B, C and D.

Based on the calculated values for the fault voltage source and fault current from the first two stages, the voltage at the fault point can be written as (10).

$$V_{x_{abc}} = V_{fault_{abc}} - R_f I_{f_{abc}} \tag{10}$$

By equating (9) and (10), and with some mathematical manipulations assuming the fault is resistive, a 3^{rd} order polynomial can be obtained to calculate the fault distance x (11).

$$A_{N_{abc}} + B_{N_{abc}} x + C_{N_{abc}} x^2 + D_{N_{abc}} x^3 = 0 \tag{11}$$

where $K_{N_{abc}} = im(K_{abc}) - re(K_{abc}) im(I_{f_{abc}})/re(I_{f_{abc}})$, $re()$ and $im()$ refers to real and imaginary parts respectively, K refers to B, C and D, and for A, $K = A - V_{fault}$.

The value of x can be used in the next iteration starting from (4), and the final value of x is obtained when the difference between successive iterations is below a pre-set threshold.

2.2. SEWIBFL scheme for a phase fault

Consider a fault between phase (a) and phase (b). The equivalent circuit at non-fundamental frequencies is shown in Fig. 3 with the fault voltage source connected between the fault phases. The analysis in this section is similar to that derived for the ground faults and only the final equations are stated to save space. The first two stages corresponding to building the fault voltage source and estimating the fault current are exactly the same using the three phase analysis. The line to line values for the fault voltage source ($V_{faultab}$) and the voltage at the fault point (V_{xab}) are given by (12). Also, the fault current is obtained in the same manner and the phase (a) fault current (I_{fa}) is considered for this fault case.

$$\begin{aligned} V_{faultab} &= V_{fault_a} - V_{fault_b} \\ V_{xab} &= V_{x_a} - V_{x_b} \end{aligned} \tag{12}$$

The final stage is to estimate the fault distance x. The procedure is followed for phase (a) and phase (b) and a 3^{rd} order polynomial has been obtained to calculate the fault distance x.

$$A_{N_{ab}} + B_{N_{ab}} x + C_{N_{ab}} x^2 + D_{N_{ab}} x^3 = 0 \tag{13}$$

where $K_{N_{ab}} = im(K_a - K_b) - re(K_a - K_b) im(I_{fa}) / re(I_{fa})$, $re()$ and $im()$ refers to real and imaginary parts respectively, K refers to B, C and D, and for A, $K = A - V_{fault}$.

For a phase to phase fault between any other two phases, the same structure as (13) can be used with the components that correspond to the fault phases. For a three-phase fault, it can be treated as three phase to phase faults and the analysis with the phase to phase is still valid. For both ground and phase faults, this three-stage procedure is repeated until the difference between two consecutive estimates is acceptable.

It is worth noting that, the method requires the pre-fault data to create the fault voltage source. For a system which has been isolated (i.e. the pre-fault data is zero) and then restored onto a fault, it will not be possible to locate this fault using the proposed method. However, the transient generated from this reconnection can be considered an active injection and an active impedance estimation technique could be used to locate such faults.

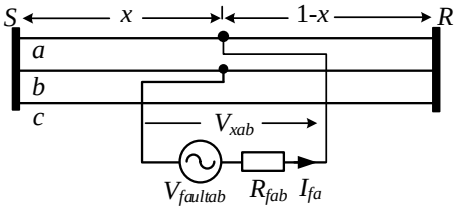

Fig. 3: SEWIBFL scheme with phase to phase fault

2.3. Data processing and root selection

The proposed scheme is a single ended method which uses measurements at the main substation only. Three-phase voltages and currents are captured with a sampling rate of 20 kHz for a period of 40 ms composed of 20 ms pre-fault and 20 ms during the fault. The captured signals are processed using frequency domain analysis to find the non-fundamental frequency components required for the fault distance estimation algorithm. The data processing includes applying a window function to remove the end effects [22], and applying the Fast Fourier Transform to find the non-fundamental components. For every frequency in the frequency range of interest, the fault distance x is calculated using either (11) or (13). A frequency range upto 3 kHz is used as it provides a good signal to noise ratio and is typical of standard instruments used for this purpose [15]. The solution of the equation leads to three roots at each frequency considered and the correct root should be real positive value and less than 1 pu. After estimating the distance over the frequency range of interest, the final distance is calculated as the average over the whole frequency range.

The main voltage source may contain low order system harmonics with small values e.g. 3^{rd} and 5^{th} harmonics. To accommodate for that, frequencies below 250 Hz were discarded from the calculations. This lower frequency border may be increased if necessary or the system harmonics can be selectively eliminated from calculation if the main system has significant higher order harmonics. Also, other sources of harmonics such as inverter based distributed generation may be present in the system. The scope of this paper does not include the effect of distributed generation. This will be considered in a future publication.

3. Applying the proposed scheme to distribution systems

Real distribution systems have loading taps and laterals. The previous derivation requires the voltage and current data at the start of the fault section and also an equivalent impedance at the end of the fault section. These two requirements are now analysed.

With measurements only available at the substation node, the voltage and current at the start of any section can be calculated by a downstream sweep along the system. Assume a section between two nodes i and j where j is downstream to i, (see Fig. 4). The measurements can be swept from i to j by (14) [21]. The current leaving node j is calculated by (15). This algorithm is recursively applied starting from the substation node.

$$\begin{bmatrix} V_j \\ I'_j \end{bmatrix} = \begin{bmatrix} \cosh(\gamma l) & -z_c \sinh(\gamma l) \\ -\sinh(\gamma l)/z_c & \cosh(\gamma l) \end{bmatrix} \begin{bmatrix} V_i \\ I_i \end{bmatrix} \tag{14}$$

$$I_j = I'_j - Y_{L(j)} V_j \tag{15}$$

where l is the length of the section ij and $Y_{L(j)}$ is the load or equivalent admittance at node j. If $Y_{L(j)}$ is not a single load e.g. a lateral with some lines and loads, the equivalent impedance needs to be calculated in a similar way to calculating Z_{eq}.

The equivalent impedance at the end of the fault section can be calculated using a recursive procedure starting from the end node of the feeder. To illustrate this, consider the system in Fig. 5, and the target is to calculate the equivalent impedance $Z_{eq(m)}$ knowing the impedance $Z_{eq(m+1)}$. The relationship between the voltage and current at the start and end of the line section is given by (16) and the relationship between the voltage and current at the end of the line section is given by (17). Substituting (17) in to (16), the equivalent impedance $Z_{eq(m)}$ can be obtained as (18).

$$\begin{bmatrix} V_m \\ I_m \end{bmatrix} = \begin{bmatrix} A_l & B_l \\ C_l & D_l \end{bmatrix} \begin{bmatrix} V_{m+1} \\ I'_{m+1} \end{bmatrix} \tag{16}$$

where $A_l = D_l = \cosh(\gamma l)$, $B_l = z_c \sinh(\gamma l)$ and $C_l = \sinh(\gamma l)/z_c$.

$$V_{m+1} = Z_{eq(m+1)} I'_{m+1} \tag{17}$$

$$Z_{eq(m)} = [Y_{L(m)} + (C_l Z_{eq(m+1)} + D_l)(A_l Z_{eq(m+1)} + B_l)^{-1}]^{-1} \tag{18}$$

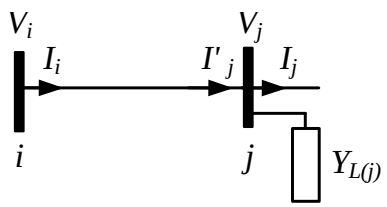

Fig. 4: Downstream sweep for measurements

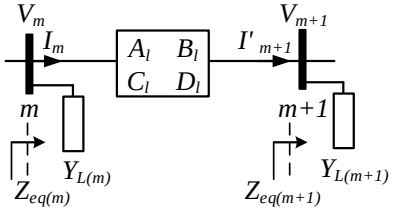

Fig. 5: Equivalent impedance calculation

As the distribution system has many line sections, the fault is located iteratively by assuming the fault is in the first section next to the substation and applying the proposed fault location method. If the estimated fault distance exceeds the total section length, the fault location method is then applied on the next section until the correct distance is calculated.

Similar to other impedance based fault location methods (and any fault location method that depends on measurements at local substation only [13]) several candidate points for a certain fault case will be presented due to the presence of laterals in the distribution system. The estimation of the exact fault section is not a part of the research in this paper and is to be studied in future work. At the moment, the proposed SEWIBFL scheme can be combined with another method to work as an integrated method such as [11] to solve the problem of multiple estimation.

4. Detection of fault inception point

As has been stated, a virtual fault voltage source is required with a step change at the fault inception point. Therefore, an algorithm to detect the fault inception point is essential. In this section, two algorithms are proposed to perform this function namely the “Second Rate of Change” method and the “Time Domain Subtraction” method. The two algorithms employ the fact that a discontinuity in the measured voltage occurs at the fault inception. Once a fault has been detected by any method e.g. current level detector, a time window that combines both pre-fault and during fault data is formed and then one of the two algorithms is used to detect the actual fault inception point in this window

4.1. Second rate of change

In order to detect the fault inception point, a parameter called the Second Rate of Change (*SRC*) at sample number (n), is calculated using three samples ($n,\ n+1$, and $n+2$) by (19).

$$SRC(n) = ||v(n) - v(n+1)| - |v(n+1) - v(n+2)|| \tag{19}$$

where $v(i)$ is the source voltage measured at sample number i.
By sweeping over the recorded voltage signal, when the fault inception point is included in the *SRC* calculation, it's value increases sharply indicating a fault inception. In (19), the fault inception point will be $(n+2)$ and the corresponding *SRC* high value will be stored at point (n) i.e. the detection appears 2 samples before the fault inception point.

4.2. Time domain subtraction

In this method, the time window that contains the fault inception point is subtracted sample by sample from a pre-fault time window of the same length. The resulting difference will have a significant value at the first fault point. In this case the window must match an integer number of fundamental cycles.

4.3. Compensating the wave propagation delay time

It is assumed the fault voltage source created has a step change at the fault inception instant. In the previous subsection, the initial reaction point in the substation voltage to the fault has been detected using two different algorithms. However, this point may be different from the actual fault inception point: for long distribution systems, the combination of line inductance and capacitance will cause a time delay during the signal propagation from the fault point to substation point [21]. Based on the line length, line parameters and fault location, this time delay may lead to a difference between the actual fault inception sample at the fault point and the reaction sample at the substation measurement point. Therefore, the estimated fault inception point in the substation voltage that has been defined in the previous subsection cannot always be used for creating the fault voltage source.

Wave propagation theory indicates that a signal takes a time to propagate from point to point along a transmission line and this is known as the propagation/travelling time, which

is dependent on the line parameters [21]. For a line with per unit length inductance and capacitance of L and C respectively, the propagation time per unit length of the line and can be calculated using (20).

$$t_d = \sqrt{LC} \tag{20}$$

Therefore, the travelling time can be calculated and considered when building the fault voltage source. As the SEWIBFL scheme assumes the fault to be in the first section next to substation and iteratively moves along the feeder until finding the fault point, the travelling time between the start node of the assumed fault section and the substation node is used to compensate for the time delay. For an incorrectly identified fault section, the travelling time will also be incorrect and will not help in finding the fault distance therefore the SEWIBFL scheme moves to the next section.

It is worth noting that it might be difficult to accurately calculate the exact travelling time for the signal moving from the fault point to the substation for various reasons:

1. As the actual fault point is unknown along the assumed fault section, it is only possible to calculate the travelling time between the start node of the fault section and the substation node. Therefore, a time error will exist if the travelling time between the actual fault point and the start node of the fault section is influential.
2. The travelling time calculated depends on the line parameters which might have a tolerance and uncertainty.

Consequently, the basic travelling time between the substation and the start of the assumed fault section is calculated using (20) and accordingly the different number of samples to be considered between the substation voltage and the step voltage source created can be found. To compensate for these potential sources of error, this estimated number of samples should be iteratively increased and/or decreased by one or two so that it reflects the actual time.

5. Simulation studies

The proposed method has been evaluated on a representative distribution system—the IEEE 34-bus feeder [20]. This feeder contains most of the common features of distribution

systems e.g. unbalanced loads, single and three-phase laterals and non-homogeneous feeder sections and has been widely used for fault location studies [3, 4]. The single line diagram for the feeder is shown in Fig. 6 and it has been simulated using the distributed line model using the Matlab/Simulink packages. The voltages and currents at the main substation have been measured with a sampling rate of 20 kHz and filtered with a low pass filter (cut-off frequency of 5 kHz). Firstly, a fault case is presented to illustrate the operation of the proposed fault inception point detectors (FIPD) and also to emphasize the signal propagation time delay. Then, the accuracy of the proposed scheme will be demonstrated for single line to ground (SLG) and phase to phase (DP) faults at different fault scenarios.

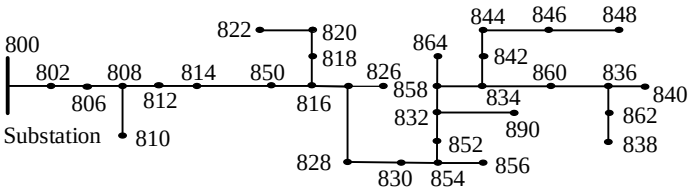

Fig. 6: Single line diagram for IEEE 34-bus feeder

5.1. Performance of fault inception point detectors

A SLG fault with a resistance of 10 Ω has been simulated at node 812. The voltage of the faulted phase has been measured and is shown in Fig. 7. As is clear from the zoomed view, the last healthy sample is 397 and the first faulty sample is 398. By applying the proposed two algorithms to detect the fault inception point, the result is illustrated in Fig. 8. For the *SRC* algorithm, once the first fault point is included in the *SRC* calculation as point $(n+2)$ in (19), the value of the *SRC* which is stored at point (n) sharply increases i.e. the *SRC* has a high value at a point which is 2 samples before the fault inception point. For this test case $n+2=398$, therefore $SRC(396)$ will have the first sharp increase. For the second algorithm, sample number 398 corresponds to the first fault sample detected with a high value.

For the same fault case, the voltage at the fault node has been measured in the simulation and is shown with the substation voltage in Fig. 9. From the figure, the first fault sample at the fault location is 396, and the first reaction for the measured substation voltage occurs at 398 which is delayed by 2 samples. This emphasizes the effect of delay due to wave

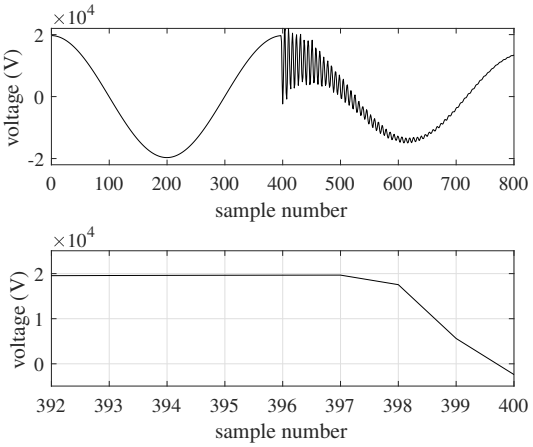

Fig. 7: Recorded voltage for a SLG fault case

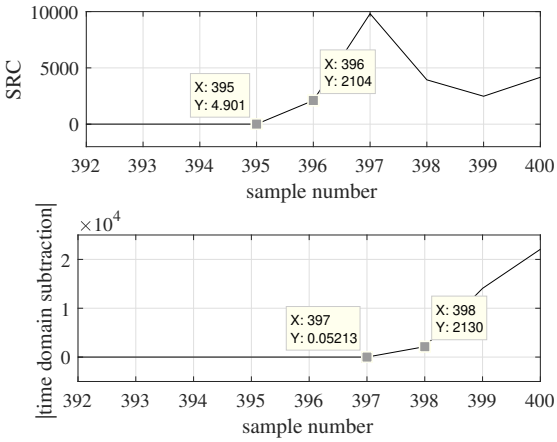

Fig. 8: Output for FIPD

propagation. For this fault case, creating the fault voltage source with a step change at the detected sample in the substation voltage becomes incorrect and leads to a high error of about 1.5 km in distance estimation. Using the parameters of the line (inductance and capacitance) that corresponds to the α mode and noting the distance between the fault node and substation is 22567 m, the travelling time is calculated as $t_d = 97$ μs. For a sampling frequency of 20 kHz, this time represents 1.94 samples which can be approximated to 2 samples. Therefore, the fault voltage source created should lead the inception point of the substation voltage by 2 samples which can clearly be seen in Fig. 9.

5.2. Performance of SEWIBFL scheme

To evaluate the performance of the proposed method, SLG and DP faults have been simulated for different scenarios. The evaluation considers changing the fault point, resistance and inception angle. Also, the effect of noise and uncertainty in the line parameters on the accuracy has been assessed. The error in the estimated distance is calculated as the absolute difference between the actual and the estimated distances. Note that the total line length of the feeder is about 93 km and the length of the longest path is about 58 km.

5.2.1. Effect of line capacitance

The system including capacitance has been simulated with faults placed at different locations. The proposed method was employed and the results are presented in Fig. 10.

For comparison with [17] that ignores the line capacitance, the results while ignoring the line capacitance are also presented, and the improvement is very clear seen.

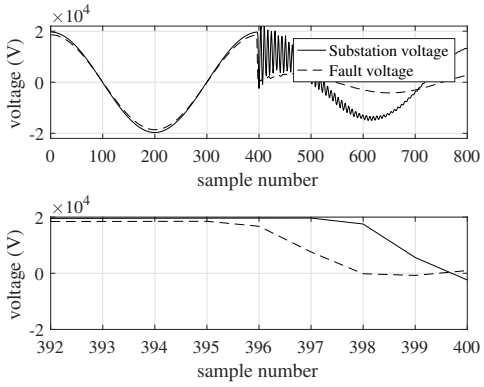

Fig. 9: Voltage at substation and fault nodes

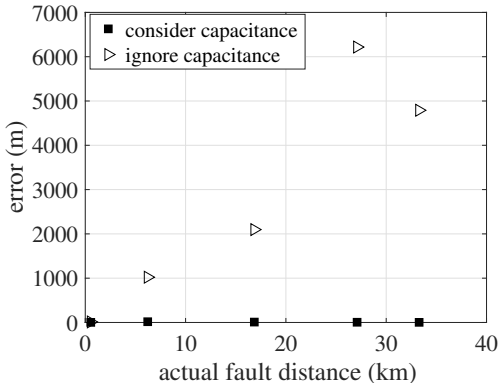

Fig. 10: Effect of ignoring the line capacitance

5.2.2. Effect of fault resistance

At different points along the system, SLG and DP faults were simulated with fault resistance values of 0.01, 1, 10 and 100 Ω. The fault inception angle is kept constant at 90°. The errors obtained for SLG and DP faults are presented in Fig. 11. Also, for further evaluation, 50 random values for the fault resistance between 0.01 Ω and 100 Ω have been created (minimum, maximum and average resistance are 4.6, 98.7 and 45.6 Ω respectively). SLG faults have been simulated with these fault resistance values in the middle of the sections between nodes (806-808), (812-814) and (858-834). These three locations lie at a distance of 6.2 km, 27 km and 55 km from the substation. The performance of the SEWIBFL scheme for this test is summarized in Table 1. In Table 1, the percentage of the fault cases which are accurate to within 50 m is given and also the average and maximum absolute error. The results show that the proposed SEWIBFL scheme provides very low error for different fault resistance values and for most of the test cases, the error is less than 50 m.

5.2.3. Effect of fault inception angle

The fault inception angle is the voltage angle at the instant of fault inception. This angle will affect the level of high frequency content in the signals processed. The absolute error is shown in Fig. 12 for both SLG and DP faults at inception angles of 5, 45, 100, 145 and

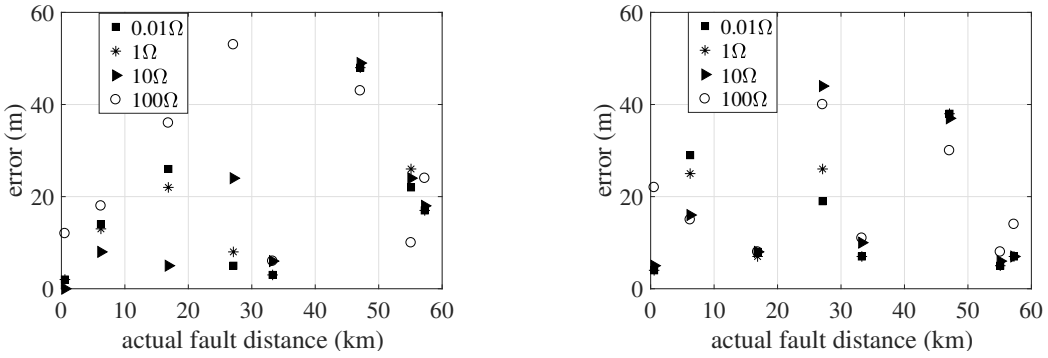

Fig. 11: Effect of fault resistance (a) SLG and (b) DP faults

160° and the fault resistance is kept as 10 Ω. Also, SLG faults at 50 random inception angles between 0° and 180° have been simulated at three locations and the results are summarized in Table 1. The SEWIBFL scheme shows a robust performance for different inception angles with a little increase in error at low fault inception angles. Also, for different cases, most of the cases introduce an error of less than 50 m and the maximum error obtained for these tests does not exceed 110 m, (refer to Fig. 12 and Table 1).

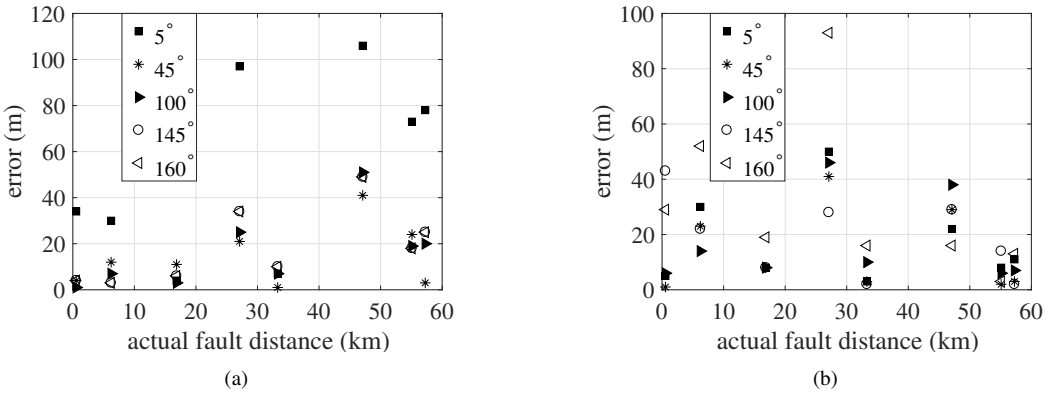

Fig. 12: Effect of inception angle (a) SLG and (b) DP faults

5.2.4. Effect of noise in measurement

The measured voltages and currents are susceptible to perturbations e.g. electromagnetic interference noise and accuracy of the measuring instruments. Gaussian noise is used to add random noise to the measured signals and a 16 bit quantizer has been added to represent the analogue to digital converter used for data capturing. For the three aforementioned line

Table 1: Performance of SEWIBFL for different fault resistances and inception angles

section	fault resistance summary			inception angle summary		
	% cases	error (m)		% cases	error (m)	
		average	maximum		average	maximum
806-808	100%	10.8	32	100%	11.6	39
812-814	92%	38.8	56	98%	26.7	110
858-834	100%	18.5	25	86%	26.3	66

sections, faults have been simulated 50 times at each location. For each fault case, the noise level is randomly selected from the range $\pm 0.1\%$ to $\pm 1\%$ of the pre-fault rms value for voltage and current while the fault resistance and inception angle were maintained constant at 1 Ω and 60° respectively. Table 2 shows the performance of the method considering the presence of noise in the measurements (percentage of cases which are accurate to within 50 m, average and maximum error). It is clear that for both SLG and DP faults, the highest percentage of cases have errors less than 50 m with a maximum error of 60 m.

Table 2: Performance of SEWIBFL for noise in measurements

section	SLG fault summary			DP fault summary		
	% cases	error (m)		% cases	error (m)	
		average	maximum		average	maximum
806-808	98%	10	52	100%	29.1	37
812-814	98%	19	56	100%	18.4	37
858-834	94%	25.4	60	98%	14.1	58

5.2.5. Uncertainty in the line parameters

Impedance based fault location methods require information about the line parameters. Uncertainty about the line parameters affects on the methods accuracy and this is unavoidable. The effect of this uncertainty is checked by assuming an error in the available line length data. Firstly, a constant error of +1% and +2% were assumed for all lines which is expected to produce a proportional increase in the estimation error. Secondly, a random error in the range $\pm 2\%$ was used for different lines. The percentage value is based on each line segment length. SLG faults were simulated at three locations and the error in the estimation is presented in Table 3 compared to the original error when using the exact line data. As expected the

estimation error increases in proportional to the increase in the line data error for the first scenario. For this IEEE feeder, it can be said that each 1% error in the calibration of the line length may lead to about 0.5% error in the distance estimation. On the other hand, when using a random error for different lines, the estimation error is smaller than the case of +2%.

Table 3: Performance of SEWIBFL for uncertainty in line parameters

distance	error in distance estimation (m)			
(km)	original	+1%	+2%	±2%
8.2	78	86	107	68
30.7	32	246	467	219
57.4	50	331	557	94

5.3. Comparison with other impedance based methods

Impedance based fault location techniques that have been tested on the same feeder (IEEE 34-bus) have been reported in [3, 4]. These techniques use analysis at the fundamental frequency and the evaluation process assumed homogeneous feeder lines (configuration # 300 [20]). The capacitive effect of the line has been considered in [4] by using a π model for the lines. In [3], the technique considered the distributed parameter model and used the sequence component networks to decouple the three phase system. However, the sequence networks will be coupled for unbalanced system [5].

The error in the estimated distance is converted from percentage to metres based on the total feeder length in [3, 4] with the aim of comparison. For different fault resistance values and different fault inception angles if applicable, the maximum errors reported in [3] are 300 m and 226 m for phase *a* to ground and phase *a* to phase *b* faults respectively. In [4], the maximum errors are 1170 m and 830 m for phase *a* to ground and phase *a* to phase *b* faults respectively. It is worth noting that the evaluation in [3] considered changing the fault inception angle and it has not been mentioned in [4]. For the proposed method, the maximum errors are 110 m and 93 m for phase *a* to ground and phase *a* to phase *b* faults respectively not including the line parameter uncertainty results. This result shows the improved accuracy of the proposed method. The error obtained by the proposed method is as good as that obtained by [3] or even a little bit better. However, it is much better than the accuracy obtained in [4].

In [4], each line section was simulated as a number of cascaded π circuits based on the length of each section. The analysis approximated the line to a single π circuit which leads to the high error in distance estimation.

The accuracy of the proposed method was also checked against [23]. The main hypothesis used in [23] is that the total fault current is in phase with the portion of the fault current flowing from the measuring end side and this may lead to high errors. When applying [23] on a simple system similar to that in Fig. 2, the error was as high as 11%.

It is worth noting that, the proposed method has been derived assuming the fault resistance is time invariant. For faults with a time varying resistance, a preliminary study shows that the proposed method can converge and estimate the fault distance but with a wider error range. However, it was not possible to include this due to space limitations. It will be discussed in a future paper.

6. Conclusions

A single end impedance based fault location technique using wideband frequency analysis has been presented. The general distributed parameter line model has been used to simulate the distribution system to consider both inductive and capacitive coupling for the line. The technique uses the available measurements at the main substation with a sampling rate of 20 kHz. As the method represents the fault by a step voltage source, algorithms to detect the fault inception sample have been presented and the effect of the wave propagation time delay has been considered. A simulation study has been conducted on the IEEE 34-bus feeder, which exhibits typical features of distribution systems e.g. unbalanced loads and non-homogeneous sections. The performance of the proposed method against single line to ground and phase to phase faults under different scenarios (e.g. changing the fault resistance, changing the fault inception angle and also adding noise to measurements) has been evaluated. The results show that the proposed method is robust and works well under different evaluation scenarios. The absolute error for most of the cases considered is less than 50 m. Noting that the total line length for the IEEE 34-bus feeder is about 93 km and length of the longest path is about 58 km, the error obtained by the proposed method becomes very low. Incorporating

distributed generation especially inverter based systems is a part of the future work to show the effectiveness of this high frequency approach.

Acknowledgment

This work is supported by the Egyptian government, ministry of higher education and the British Council through Newton-Mosharafa scholarships.

References

[1] House of Commons, Energy and Climate Change Committee, 2020 renewable heat and transport targets (Sep. 2016).
URL https://publications.parliament.uk/pa/cm201617/cmselect/cmenergy/173/173.pdf

[2] M. M. Saha, J. J. Izykowski, E. Rosolowski, Fault location on power networks, Springer Science & Business Media, 2009 (2009).

[3] R. Dashti, J. Sadeh, Accuracy improvement of impedance-based fault location method for power distribution network using distributed-parameter line model, International Transactions on Electrical Energy Systems 24 (3) (2014) 318–334 (2014). doi:10.1002/etep.1690.

[4] R. H. Salim, K. C. O. Salim, A. S. Bretas, Further improvements on impedance-based fault location for power distribution systems, IET Generation, Transmission & Distribution 5 (4) (2011) 467–478 (2011). doi:10.1049/iet-gtd.2010.0446.

[5] M. Choi, S. Lee, S. Lim, D. Lee, X. Yang, A direct three-phase circuit analysis-based fault location for line-to-line fault, IEEE Transactions on Power Delivery 22 (4) (2007) 2541–2547 (2007).

[6] A. Bahmanyar, S. Jamali, Fault location in active distribution networks using non-synchronized measurements, International Journal of Electrical Power & Energy Systems 93 (2017) 451 – 458 (2017). doi:10.1016/j.ijepes.2017.06.018.

[7] S. Lotfifard, M. Kezunovic, M. J. Mousavi, Voltage sag data utilization for distribution fault location, IEEE Transactions on Power Delivery 26 (2) (2011) 1239–1246 (2011).

[8] D. W. P. Thomas, R. J. O. Carvalho, E. T. Pereira, Fault location in distribution systems based on traveling waves, in: IEEE Bologna Power Tech Conference Proceedings, 2003 (2003).

[9] M. Goudarzi, B. Vahidi, R. Naghizadeh, S. Hosseinian, Improved fault location algorithm for radial distribution systems with discrete and continuous wavelet analysis, International Journal of Electrical Power & Energy Systems 67 (2015) 423 – 430 (2015).

[10] J. J. Mora, G. Carrillo, L. Perez, Fault location in power distribution systems using ANFIS Nets and current patterns, in: IEEE/PES Transmission & Distribution Conference and Exposition: Latin America, 2006 (2006).

[11] F. C. Trindade, W. Freitas, Low voltage zones to support fault location in distribution systems with smart meters, IEEE Transactions on Smart Grid 8 (6) (2017) 2765–2774 (2017).

[12] R. Dashti, J. Sadeh, Fault section estimation in power distribution network using impedance-based fault distance calculation and frequency spectrum analysis, IET Generation, Transmission & Distribution 8 (8) (2014) 1406–1417 (2014).

[13] A. Bahmanyar, S. Jamali, A. Estebsari, E. Bompard, A comparison framework for distribution system outage and fault location methods, Electric Power Systems Research 145 (2017) 19–34 (2017). doi:10.1016/j.epsr.2016.12.018.

[14] J. Mora-Flòrez, J. Meléndez, G. Carrillo-Caicedo, Comparison of impedance based fault location methods for power distribution systems, Electric Power Systems Research 78 (4) (2008) 657–666 (2008). doi:10.1016/j.epsr.2007.05.010.

[15] K. Jia, D. Thomas, M. Sumner, A new single-ended fault-location scheme for utilization in an integrated power system, IEEE Transactions on Power Delivery 28 (1) (2013) 38–46 (2013). doi:10.1109/TPWRD.2012.2215346.

[16] K. Jia, D. W. P. Thomas, M. Sumner, A new double-ended fault-location scheme for utilization in integrated power systems, IEEE Transactions on Power Delivery 28 (2) (2013) 594–603 (2013). doi:10.1109/TPWRD.2013.2238560.

[17] K. Jia, T. Bi, Z. Ren, D. Thomas, M. Sumner, High frequency impedance based fault location in distribution system with DGs, IEEE Transactions on Smart Grid 9 (2) (2018) 807–816 (2018).

[18] F. M. Aboshady, M. Sumner, D. W. P. Thomas, A double end fault location technique for distribution systems based on fault-generated transients, in: IEEE 26th International Symposium on Industrial Electronics (ISIE), 2017, pp. 32–36 (2017). doi:10.1109/ISIE.2017.8001219.

[19] F. M. Aboshady, D. W. P. Thomas, M. Sumner, Fast fault location scheme for distribution systems based on fault transients, in: International Conference on Resilience of Transmission and Distribution Networks, IET, 2017 (2017). doi:10.1049/cp.2017.0327.

[20] IEEE PES AMPS DSAS Test Feeder Working Group, 34-bus feeder.
URL `http://sites.ieee.org/pes-testfeeders/resources/`

[21] J. J. Grainger, W. D. Stevenson, G. W. Chang, Power system analysis, McGraw-Hill New York, 1994 (1994).

[22] A. V. Oppenheim, R. W. Schafer, Discrete-Time Signal Processing, 3rd Edition, Prentice Hall Press, Upper Saddle River, NJ, USA, 2009 (2009).

[23] T. Takagi, Y. Yamakoshi, M. Yamaura, R. Kondow, T. Matsushima, Development of a new type fault locator using the one-terminal voltage and current data, IEEE Transactions on Power Apparatus and Systems PAS-101 (8) (1982) 2892–2898 (1982).